DOI: 10.1021/ic100343t

Inorganic Chemistry
Article

On the Origin of the Inverted Stability Order of the Reverse-Keggin $[(MnO_4)(CH_3)_{12}Sb_{12}O_{24}]^{6-}$: A DFT Study of α, β, γ, δ, and ε Isomers

Fu-Qiang Zhang,[†] Wei Guan,[‡] Yin-Tang Zhang,[†] Mao-Tian Xu,*[,†] Jian Li,[†] and Zhong-Min Su*[,‡]

[†]*Department of Chemistry, Shangqiu Normal University, Shangqiu 476000, People's Republic of China, and* [‡]*Institute of Functional Material Chemistry, Department of Chemistry, Northeast Normal University, Changchun 130024, People's Republic of China*

Received February 20, 2010

Density functional theory calculations have been carried out to investigate the α, β, γ, δ, and ε isomers of $[(MnO_4)Me_{12}Sb_{12}O_{24}]^{6-}$ (Me = CH_3) anions, which are simplified Baker−Figgis models of Keggin-type antimonate complexes in experiments. It is found that the stability order of the five isomers (α < β < γ < δ < ε) perfectly reverses to the well-known trend of the classical Keggin $[PW_{12}O_{40}]^{3-}$ anions (α > β > γ > δ > ε), despite their significant similarities in frameworks. On the basis of the building block decomposition method, the stabilizing effect of the edge-sharing $[Sb_2(\mu\text{-}O)_2Me_2]$ fragment inside γ, δ, and ε structures is confirmed and found to originate from its two energy-favorable components rather than itself as an indivisible unit. Similar behavior is also held by the destabilizing $[W_2(\mu\text{-}O)_2O_2]$ fragment in $[PW_{12}O_{40}]^{3-}$; however, the well-accepted electrostatic repulsion between the short W^{VI}−W^{VI} contacts cannot be taken as direct evidence. Notably, in the assembly of the $[(MnO_4)Me_{12}Sb_{12}O_{24}]^{6-}$ structure, all of the octahedral building units incline to compress axially and elongate horizontally, and this is exactly opposite to the deformation pattern observed in the building blocks of Keggin tungstates, which tend to elongate axially and compress horizontally, thus giving rise to the inverted stability order. Furthermore, energy decomposition analysis reveals that the intrinsic property of the anion comes from the spatial arrangements of the metal−oxygen cage and does not change significantly with the type and charge of the encapsulated anion.

Introduction

The Keggin anion,[1] the most prominent representative of the polyoxometalates (POMs), is known for a range of M (Mo, W, V, etc.) and a wider range of heteroatom X (S, P, As, Si, Ge, B, Al, Ga, etc.).[2] In 1970, Baker and Figgis[3] predicted the existence of five possible isomers with names of α, β, γ, δ, and ε, which differ in the arrangement of the metal oxide core and in symmetry. In most cases, the p-block element X is surrounded by four tetrahedral oxygen atoms (XO_4) at the inner cavity of a spherical metal−oxygen shell ($M_{12}O_{36}$) arranged by 12 d-block metals.

The Keggin anions are preferred to adopt α and β forms, especially the most stable α one (α > β), whereas the γ, δ, and ε frameworks are thermodynamically unstable.[4−6] Kepert and Pope[4] originally proposed that the edge-sharing $[M_2(\mu\text{-}O)_2O_2]$ subunits played a crucial rule in destabilizing the later three structures (ε < δ < γ), arising from the electrostatic repulsion between the short M−M contact. This viewpoint has been partly confirmed by the recent theoretical work of López and Poblet.[7] Notably, the δ and ε structures seem to become stable when all 12 transition metals are (i) one-electron-reduced (5+ oxidation state) or (ii) substituted by main-group metals with low valence,[8] as exhibited by increasing experimental evidence such as complexes with an ε-Mo^{V}_{13} core,[9] ε-MAl_{12} (M = Al^{III},

*To whom correspondence should be addressed. E-mail: zmsu@nenu.edu.cn (Z.-M.S.), xumaotian@sqnc.edu.cn (M.-T.X.). Tel/Fax: +8603702595593. Fax: +8603702595593.

(1) Keggin, J. F. *Nature* **1933**, *131*, 908–909.
(2) For example, see:Pope, M. T. *Heteropoly and Isopolyoxometalates*; Springer-Verlag: Berlin, 1983; p 26.
(3) Baker, L. C. W.; Figgis, J. S. *J. Am. Chem. Soc.* **1970**, *92*, 3794–3797.
(4) (a) Kepert, D. L. *Inorg. Chem.* **1969**, *8*, 1556–1558. (b) Pope, M. T. *Inorg. Chem.* **1976**, *15*, 2008–2010.
(5) Tezé, A.; Hervé, G. *J. Inorg. Nucl. Chem.* **1977**, *39*, 2151–2154.
(6) (a) Weinstock, I. A.; Cowan, J. J.; Barbuzzi, E. M. G.; Zeng, H.; Hill, C. L. *J. Am. Chem. Soc.* **1999**, *121*, 4608–4617. (b) Neiwert, W. A.; Cowan, J. J.; Hardcastle, K. I.; Hill, C. L.; Weinstock, I. A. *Inorg. Chem.* **2002**, *41*, 6950–6952. (c) Sundaram, K. M.; Neiwert, W. A.; Hill, C. L.; Weinstock, I. A. *Inorg. Chem.* **2006**, *45*, 958–960.
(7) López, X.; Poblet, J.-M. *Inorg. Chem.* **2004**, *43*, 6863–6865.
(8) The M_{13} (M = Fe^{III}, Cr^{III}) suggested but never structurally substantiated are not included. For example, see: (a) Bradley, S. M.; Kydd, R. A. *J. Chem. Soc., Dalton Trans.* **1993**, 2407–2413. (b) Bradley, S. M.; Lehr, C. R.; Kydd, R. A. *J. Chem. Soc., Dalton Trans.* **1993**, 2415–2420.
(9) For example, see: (a) Khan, M. I.; Zubieta, J. *J. Am. Chem. Soc.* **1992**, *114*, 10058–11509. (b) Khan, M. I.; Müller, A.; Dillinger, S.; Bögge, H.; Chen, Q.; Zubieta, J. *Angew. Chem., Int. Ed. Engl.* **1993**, *32*, 1780–1782. (c) Khan, M. I.; Chen, Q.; Salta, J.; O'Connor, C. J.; Zubieta, J. *Inorg. Chem.* **1996**, *35*, 1880–1901. (d) Müller, A.; Dillinger, S.; Krickemeyer, E.; Bögge, H.; Plass, W.; Stammler, A.; Haushalter, R. C. *Z. Naturforsch.* **1997**, *52b*, 1301–1306. (e) Müller, A.; Meyer, J.; Krickemeyer, E.; Beugholt, C.; Bögge, H.; Peters, F.; Schmidtmann, M.; Kögerler, P.; Koop, M. J. *Chem.—Eur. J.* **1998**, *4*, 1000–1006. (f) Bereau, V.; Cadot, E.; Bögge, H.; Müller, A.; Sécheresse, F. *Inorg. Chem.* **1999**, *38*, 5803–5808. (g) Müller, A.; Beugholt, C.; Kögerler, P.; Bögge, P.; Buiko, S.; Luban, M. *Inorg. Chem.* **2000**, *39*, 5176–5177. (h) Ueda, T.; Yonemura, T.; Shiro, M.; Fukudome, M.; Hojo, M. *Inorg. Chem. Commun.* **2007**, *10*, 1301–1303.

Published on Web 05/25/2010

Ge^{IV}, Ga^{III}),[10] ε-Ga_{13},[11] and δ-Al_{13}[12] and antimonites with an ε/δ-{$MnSb_{12}$} core.[13] The adoption of the ε or δ framework rather than the α or β one indicates that the nature of these species is distinct from that of the traditional Keggin POMs. In case i, the complex is built of dicationic $[M^{V}_2(\mu\text{-}X)_2O_2]^{2+}$ (M = Mo, W; X = O, S) units, in which the very short M−M distance and diamagnetic behavior in the experiment[14] and the strong localization of its frontier molecular orbital (FMO) in theory[15] are combined to confirm the formation of a metallic bond between the two reduced d^1 centers. On the basis of density functional theory (DFT), our group further clarified that the very stable ε-Mo^{V}_{13} core stemmed from this kind of single-bonded binuclear fragment.[16] In contrast to case i, no metal−metal bond is observed in the low-valence-metal case ii, where it is generally thought that the electrostatic repulsion inside the edge-sharing fragment could be lowered as a result of a decrease of the metal ion charge.[17] Evidently, the lowering of the electrostatic repulsion is not a sufficient but necessary condition, and the reason that underlies the preferred formation of the ε or δ structure of these complexes is unclear.

Thanks to the development of DFT methods and computer techniques, high-level calculations of large metal systems such as POMs can be carried out more recently.[18] For the Keggin anions, great efforts have been made in rationalizing their fundamental properties such as redox, acidic, magnetic, spectroscopic, etc.[19] In contrast, much less fundamental research is devoted to the non-POM analogues.[20] Inspired by the synthetic work of Winpenny and co-workers,[13] we are interested in the structure and stability of the antimonates with reverse p- and d-block elements. $PhSbO_3H_2$ can assemble δ and ε Keggin ions in the presence of hydrated Mn^{II} or Zn^{II}. However, can it form other Keggin types? Are α, β, and γ frameworks of these species stable? What is the key factor in controlling the formation of these kinds of compounds? In this paper, we try to address these problems by DFT studies on the five Keggin-type isomers of $[(MnO_4)Me_{12}Sb_{12}O_{24}]^{6-}$ (Me = CH_3). A systematic comparison to the classical Keggin anions has been made, which sheds insight into the basic properties of the inorganic antimonite as well as other non-POM species.

Computational Details

All of the calculations were carried out with the *ADF2008.01* suite of programs.[21] At the gradient-corrected DFT level of theory, the exchange functional of modified Perdew−Wang (mPW),[22] in conjunction with the correlation functional of Perdew−Wang (PW91),[23] was used. The basis functions for describing the valence electrons of each atom are triple-ξ plus polarization Slater basis sets, which are standard TZP basis sets in the *ADF* package. The core shells, including $(1s)^2$ of C, O, and F, $(1s2s2p)^{10}$ of P and Mn, $(1s2s2p3s3p3d4s4p)^{36}$ of Sb, and $(1s2s2p3s3p3d4s4p4d)^{46}$ of W, were kept frozen and described by means of single Slater functions. The zero-order regular approximation (ZORA)[24] was adopted in all of the calculations to account for the scalar relativistic effect. Full geometry optimizations were carried out on each complex, and spin-unrestricted calculations with $S = {}^5/_2$ were performed for all of the open-shell systems. The value of the numerical integration parameter used to determine the precision of numerical integrals was 5.5. In addition, to further interpret the bonding character between the octahedral metal ion and C/O ligand, a natural bond orbital (NBO) calculation based on the optimized geometries was performed using *Gaussian 03* programs,[25] with the B3LYP functional and the 6-31G(d) basis set for carbon, hydrogen, oxygen, and phosphorus and the LANL2DZ[26] pseudopotential and basis set for manganese, zinc, tungsten, and tin. For tin, one d-type polarization function and one p-type diffuse function were also added (LANL2DZp).[27] Throughout this paper, a shorthand notation for Keggin-type structures without oxygen, carbon, and hydrogen atoms, charge, and brackets is used, e.g., PW_{12} for $[(PO_4)W_{12}O_{36}]^{3-}$, $MnSb_{12}$ for $[(MnO_4)Me_{12}Sb_{12}O_{24}]^{6-}$, etc.

(10) For example, see: (a) Johansson, G. *Acta Chem. Scand.* **1960**, *14*, 771–773. (b) Bradley, S. M.; Kydd, R. A.; Fyfe, C. A. *Inorg. Chem.* **1992**, *31*, 1181–1185. (c) Casey, W. H. *Chem. Rev.* **2006**, *106*, 1. (d) Bi, S.; Wang, C.; Cao, Q.; Zhang, C. *Coord. Chem. Rev.* **2004**, *248*, 441–455. (e) Stewart, T. A.; Trudell, D. E.; Alam, T. M.; Ohlin, C. A.; Lawler, C.; Casey, W.; Jett, S.; Nyman, M. *Environ. Sci. Technol.* **2009**, *43*, 5416–5422.

(11) (a) Bradley, S. M.; Kydd, R. A.; Yamdagni, R. *J. Chem. Soc., Dalton Trans.* **1990**, 413–417. (b) Bradley, S. M.; Kydd, R. A.; Yamdagni, R. *J. Chem. Soc., Dalton Trans.* **1990**, 2653. (c) Michot, L. J.; Montargès-Pelletier, E.; Lartiges, B. S.; de la Caillerie, J. B. D.; Briois, V.; Briois, V. E. *J. Am. Chem. Soc.* **2000**, *122*, 6048–6056.

(12) Allouche, L.; Gérardin, C.; Loiseau, T.; Férey, G.; Taulelle, F. *Angew. Chem., Int. Ed.* **2000**, *39*, 511–514.

(13) Baskar, V.; Shanmugam, M.; Helliwell, M.; Teat, S. J.; Winpenny, R. E. P. *J. Am. Chem. Soc.* **2007**, *129*, 3042–3043.

(14) (a) Compain, J.-D.; Dolbecq, A.; Marrot, J.; Mialane, P.; Sécheresse, F. *C. R. Chimie* **2010**, *13*, 329–335. (b) Cadot, E.; Sécheresse, F. *Chem. Commun.* **2002**, 2189–2197. (c) Sécheresse, F.; Dolbecq, A. *J. Solid State Chem.* **2000**, *152*, 78–86.

(15) (a) Jamet, H.; Borshch, S. *New J. Chem.* **2004**, *28*, 490–494. (b) Rohmer, M.-M.; Bénard, M.; Cadot, E.; Sécheresse, F. In *Polyoxometalate Chemistry*; Pope, M. T., Müller, A., Eds.; Kluwer Academic Publishers: Dordrecht, The Netherlands, 2001; pp 117−133.

(16) Zhang, F.-Q.; Zhang, X.-M.; Wu, H.-S.; Li, Y.-W.; Jiao, H. *J. Phys. Chem. A* **2007**, *111*, 1683–1687.

(17) Bino, A.; Ardon, M.; Lee, D.; Spingler, B.; Lippard, S. J. *J. Am. Chem. Soc.* **2002**, *124*, 4578–4579.

(18) (a) Poblet, J. M.; López, X.; Bo, C. *Chem. Soc. Rev.* **2003**, *32*, 297–308. (b) Davidson, E. R. *Chem. Rev.* **2000**, *100*, 351–352. (c) Rohmer, M.-M.; Bénard, M.; Blaudeau, J.-P.; Maestre, J.-M.; Poblet, J.-M. *Coord. Chem. Rev.* **1998**, *178*−*180*, 1019–1049.

(19) For example, see: (a) López, X.; Maestre, J. M.; Bo, C.; Poblet, J.-M. *J. Am. Chem. Soc.* **2001**, *123*, 9571–9576. (b) Maestre, J. M.; López, X.; Bo, C.; Poblet, J.-M.; Casan-Pastor, N. *J. Am. Chem. Soc.* **2001**, *123*, 3749–3758. (c) López, X.; Bo, C.; Poblet, J.-M. *J. Am. Chem. Soc.* **2002**, *124*, 12574–12582. (d) Bridgeman, A. J. *Chem.—Eur. J.* **2004**, *10*, 2935–2941. (e) de Visser, S. P.; Kumar, D.; Neumann, R.; Shaik, S. *Angew. Chem., Int. Ed.* **2004**, *43*, 5661–5665. (f) Bagno, A.; Bonchio, M. *Angew. Chem., Int. Ed.* **2005**, *44*, 2023–2026. (g) Kumar, D.; Derat, E.; Khenkin, A. M.; Neumann, R.; Shaik, S. *J. Am. Chem. Soc.* **2005**, *127*, 17712–17718. (h) Ganapathy, S.; Fournier, M.; Paul, J. F.; Delevoye, L.; Guelton, M.; Amoureux, J. P. *J. Am. Chem. Soc.* **2002**, *124*, 7821–7828. (i) Janik, M. J.; Davis, R. J.; Neurock, M. *J. Am. Chem. Soc.* **2005**, *127*, 5238–5245. (j) Yang, J.; Janik, M. J.; Ma, D.; Zheng, A.; Zhang, M.; Neurock, M.; Davis, R. J.; Ye, C.; Deng, F. *J. Am. Chem. Soc.* **2005**, *127*, 18274–18280. (k) Janik, M. J.; Bardin, B. B.; Davis, R.; Neurock, M. *J. Phys. Chem. B* **2006**, *110*, 4170–4178. (l) Guan, W.; Yang, G.; Yan, L.; Su, Z.-M. *Inorg. Chem.* **2006**, *45*, 7864–7868.

(20) (a) Qian, Z.; Feng, H.; Yang, W.; Bi, S. *J. Am. Chem. Soc.* **2008**, *130*, 14402–14403. (b) Evans, R. J.; Rustad, J. R.; Casey, W. H. *J. Phys. Chem. A* **2008**, *112*, 4125–4140. (c) Hanauer, H.; Puchta, R.; Clark, T.; van Eldik, R. *Inorg. Chem.* **2007**, *46*, 1112–1122. (d) Stack, A. G.; Rustad, J. R.; Casey, W. H. *J. Phys. Chem. B* **2005**, *109*, 23771–23775. (e) Pophristic, V.; Balagurusamy, V. S. K.; Klein, M. L. *Phys. Chem. Chem. Phys.* **2004**, *6*, 919–923.

(21) (a) te Velde, G.; Bickelhaupt, F. M.; Baerends, E. J.; Fonseca Guerra, C.; van Gisbergen, S. J. A.; Snijders, J. G.; Ziegler, T. *J. Comput. Chem.* **2001**, *22*, 931–967. (b) Fonseca Guerra, C.; Snijders, J. G.; te Velde, G.; Baerends, E. J. *Theor. Chem. Acc.* 1998, *99*, 391−403. ADF 2008. 01; SCM, Vrije Universiteit: Amsterdam, The Netherlands, 2008.

(22) Adamo, C.; Barone, V. *J. Chem. Phys.* **1998**, *108*, 664–675.

(23) Perdew, J. P.; Chevary, J. A.; Vosko, S. H.; Jackson, K. A.; Pederson, M. R.; Singh, D. J.; Fiolhais, C. *Phys. Rev. B* **1992**, *46*, 6671–6687.

(24) (a) van Lenthe, E.; Baerends, E. J.; Snijders, J. G. *J. Chem. Phys.* **1993**, *99*, 4597–4610. (b) van Lenthe, E.; Baerends, E. J.; Snijders, J. G. *J. Chem. Phys.* **1994**, *101*, 9783–9792. (c) van Lenthe, E.; Snijders, J. G.; Baerends, E. J. *J. Chem. Phys.* **1996**, *105*, 6505–6515. (d) van Lenthe, E.; van Leeuwen, R.; Baerends, E. J.; Snijders, J. G. *Int. J. Quantum Chem.* **1996**, *57*, 281–293. (e) van Lenthe, E.; Ehlers, A. E.; Baerends, E. J. *J. Chem. Phys.* **1999**, *110*, 8943–8953.

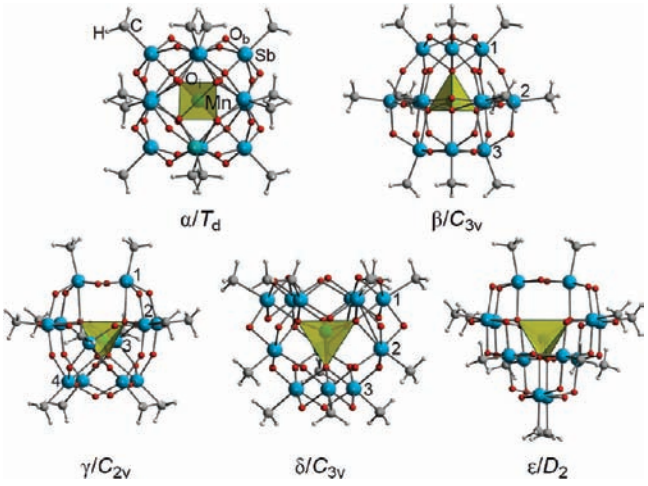

Figure 1. Ball-and-stick representations of the α, β, γ, δ, and ε [(MnO_4)-$Me_{12}Sb_{12}O_{24}]^{6-}$ isomers. Two types of oxygen atoms are given: interior (O_i) and bridging (O_b). The numbers denote different kinds of octahedral building units in the structure.

Results and Discussion

Structure. The five isomers of $MnSb_{12}$ derived from five classical Baker−Figgis[3] cap-rotation Keggin-type anions are simplified model compounds of the possible isomeric forms of the ε/δ-Keggin antimonite core,[13] in which all 12 terminal phenyl groups are substituted by methyl groups for computational convenience. The most stable structures are shown in Figure 1, and the important parameters are provided in Table 1. Our calculation shows the α/T_d, β/C_{3v}, γ/C_{2v}, and δ/C_{3v} isomers manifesting their ideal symmetries as observed in the Keggin tungstates,[7] while the ε isomer reduces from T_d to D_2 symmetry because of the slight skeleton deformation induced by orientations of the terminal methyl groups. However, the unperceivable structural deviation and the subtle energy difference (~0.10 kcal/mol) exhibit that the ε form is actually T_d-symmetric.

The four interior μ_4-O_i atoms span the inner cavity of the $MnSb_{12}$ anions (Figure 1). As listed in Table 1, both the Mn−O_i and Sb−O_i bonds are generally elongated from the α to ε isomer, which exhibits a substantial increase of the size of the anions. This behavior can be confirmed by two important parameters, the distances of X(Mn)−M(Sb) as well as the sum of the X(Mn)−O_i and M(Sb)−O_i bond lengths, which is often used to characterize the structures of the α and β Keggin anions.[6,28] As shown in Figure 2, both parameters exhibit the same stretching pattern ($\alpha < \beta < \gamma < \delta < \varepsilon$) despite their differences in ranges (3.588−3.813 and 4.144−4.345 Å for Mn−Sb and the sum on average, respectively), and their similar variation suggests that there is a ~0.2 Å expansion in size from α to ε. Moreover, inside all of the structures, the Sb−O_i (2.206−2.271 Å) is always the weakest bond with a bond order of 0.23−0.30 (Mayer index in Table SI1 in the Supporting Information, SI), reflecting that the outer neutral $Me_{12}Sb_{12}O_{24}$ (Me = CH_3) cage and the inner MnO_4^{6-} subunit are generally separated, partly in accordance with the classical host−guest complex.[29]

The bridging oxygen atoms (O_b) can be put into three categories, i.e., inside the $\{(MeSb)_3O_6\}$[30] triad (*intratriad*), between the neighboring $\{(MeSb)_3O_6\}$ triads (*intertriad*), and inside the edge-sharing $[Sb_2(\mu\text{-}O)_2Me_2]$ dumbbell (*dumbbell*). Voronoi charge analysis (Table SI2 in the SI) shows that the interior and *dumbbell* oxygen atoms always bear the largest and least negative charges (−1.317 to −1.367 and −1.205 to −1.213, respectively) and the *intertriad* oxygen atoms carry more negative charge than the *intratriad* ones (−1.229 to −1.258 vs −1.207 to −1.245). Despite being disfavored in charge, the *dumbbell* oxygen atoms in the ε or δ structure are favored to coordinate additional metal ions because of their suitable spatial arrangement in the surface of the cluster.[13] Similar to the oxygen atoms, Voronoi charges of metal ions are also less than their formal oxidation states. However, the calculated 1.368−1.388 of Mn^{II} is less than half that of 2.812−2.856 of Sb^V, in line with the chemical intuition. Interestingly, going from the α to ε isomer, the charge of Mn^{II} exhibits an increasing trend (from 1.368 to 1.388), while that of the surrounding tetrahedral O_i shows a decreasing one (from −1.351 to −1.317 on average). Consequently, the charge transferring from the MnO_4^{6-} guest to the neutral $Me_{12}Sb_{12}O_{24}$ host is substantially increased in the order $\alpha < \beta < \gamma < \delta < \varepsilon$ (~0.15e). In addition, orbital analysis exhibits that the highest occupied molecular orbitals of $MnSb_{12}$ mainly come from the half-occupied orbitals of MnO_4^{6-}; i.e., the five single electrons still strongly locate at the center Mn^{II} (e.g., $e^2t_2^3$ of the ε/T_d structure in Figure 3) and thus yield high-spin structures (Mulliken spin charge of 4.692−4.841; Table SI3 in the SI), in well agreement within the experiment.[13]

In view of the similar coordination patterns (six-coordinate) and the very close ionic radii[31] of Sb^{5+} (0.60 Å) and W^{6+}/Mo^{6+} (0.60 Å) and the same building principle of the two kinds of anions (assembly of 12 octahedra sharing their corners/edges around a central XO_4 tetrahedron), the $MnSb_{12}$ anions fully resemble the Keggin POMs, for instance, the classical $[PW_{12}O_{40}]^{3-}$,[1] in structure. However, a detailed analysis shows that there are

(25) Frisch, M. J.; Trucks, G. W.; Schlegel, H. B.; Scuseria, G. E.; Robb, M. A.; Cheeseman, J. R.; Montgomery, J. A., Jr.; Vreven, T.; Kudin, K. N.; Burant, J. C.; Millam, J. M.; Iyengar, S. S.; Tomasi, J.; Barone, V.; Mennucci, B.; Cossi, M.; Scalmani, G.; Rega, N.; Petersson, G. A.; Nakatsuji, H.; Hada, M.; Ehara, M.; Toyota, K.; Fukuda, R.; Hasegawa, J.; Ishida, M.; Nakajima, T.; Honda, Y.; Kitao, O.; Nakai, H.; Klene, M.; Li, X.; Knox, J. E.; Hratchian, H. P.; Cross, J. B.; Adamo, C.; Jaramillo, J.; Gomperts, R.; Stratmann, R. E.; Yazyev, O.; Austin, A. J.; Cammi, R.; Pomelli, C.; Ochterski, J. W.; Ayala, P. Y.; Morokuma, K.; Voth, G. A.; Salvador, P.; Dannenberg, J. J.; Zakrzewski, V. G.; Dapprich, S.; Daniels, A. D.; Strain, M. C.; Farkas, O.; Malick, D. K.; Rabuck, A. D.; Raghavachari, K.; Foresman, J. B.; Ortiz, J. V.; Cui, Q.; Baboul, A. G.; Clifford, S.; Cioslowski, J.; Stefanov, B. B.; Liu, G.; Liashenko, A.; Piskorz, P.; Komaromi, I.; Martin, R. L.; Fox, D. J.; Keith, T.; Al-Laham, M. A.; Peng, C. Y.; Nanayakkara, A.; Challacombe, M.; Gill, P. M. W.; Johnson, B.; Chen, W.; Wong, M. W.; Gonzalez, C.; Pople, J. A. *Gaussian 03*, revision C.02; Gaussian, Inc.: Pittsburgh, PA, **2003**.
(26) (a) Hay, P. J.; Wadt, W. R. *J. Chem. Phys.* **1985**, *82*, 270–283. (b) Wadt, W. R.; Hay, P. J. *J. Chem. Phys.* **1985**, *82*, 284–298. (c) Hay, P. J.; Wadt, W. R. *J. Chem. Phys.* **1985**, *82*, 299–310.
(27) Check, C. E.; Faust, T. O.; Bailey, J. M.; Wright, B. J.; Gilbert, T. M.; Sunderlin, L. S. *J. Phys. Chem. A* **2001**, *105*, 8111–8116.
(28) Zhang, F.-Q.; Zhang, X.-M.; Wu, H.-S.; Li, Y.-H.; Jiao, H. *J. Phys. Chem. A* **2007**, *111*, 159–166.
(29) (a) Müller, A.; Reuter, H.; Dillinger, S. *Angew. Chem., Int. Ed. Engl.* **1995**, *34*, 2328–2361. (b) Cooper, G. J. T.; Long, D.-L.; Bögger, H.; Müller, A.; Streb, C.; Cronin, L. *Science* **2010**, *327*, 72–74.
(30) Corresponds to the trimetallic $\{M_3O_9\}$ group in the Keggin POMs.
(31) *Lange's Handbook of Chemistry*; Dean, J. A., Ed.; McGraw-Hill Book Co.: New York, 1985.

Table 1. Selected Distances and Bond Lengths[a] (in Angstroms) for the Five $[(MnO_4)Me_{12}Sb_{12}O_{24}]^{6-}$ Isomers

anions	Mn−O_i	Sb−O_i	Sum[b]	Mn−Sb[b]	Sb−C	Sb−O_b
α/T_d	1.932	2.212	4.144	3.588	2.223	2.049−2.070
β/C_{3v}	1.931−1.945	2.202−2.215	4.148	3.589	2.219−2.224	2.046−2.071
γ/C_{2v}	1.951−1.987	2.187−2.291	4.183	3.631	2.215−2.240	2.039−2.069
δ/C_{3v}	1.997−2.062	2.176−2.285	4.247	3.699	2.214−2.238	2.039−2.066
expt[c]	2.07−2.12	2.06−2.15	4.13−4.27	3.47−3.70	2.102−2.137	1.96−2.03
ε/D_2	2.083	2.271	4.345	3.812	2.236	2.047−2.051
ε/T_d	2.083	2.271	4.345	3.813	2.236	2.047−2.051
expt[c]	2.07−2.09	2.14−2.18	4.21−4.27	3.68−3.73	2.102−2.126	1.96−2.02

[a] Observed intervals are given. [b] Averaged data are given. [c] X-ray data of δ and ε $[(MnO_4)(Ph)_{12}Sb_{12}O_{24}]^{6-}$ cores from ref 13.

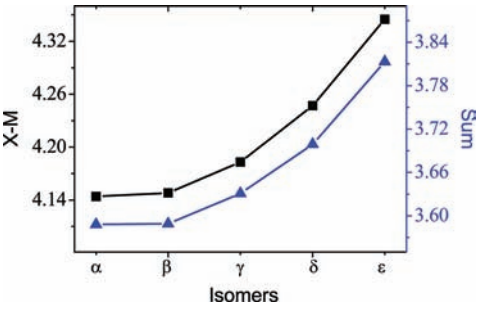

Figure 2. Distances of Mn−Sb and the sum of Mn−O_i and Sb−O_i bond lengths (Å) of five $[(MnO_4)Me_{12}Sb_{12}O_{24}]^{6-}$ isomers.

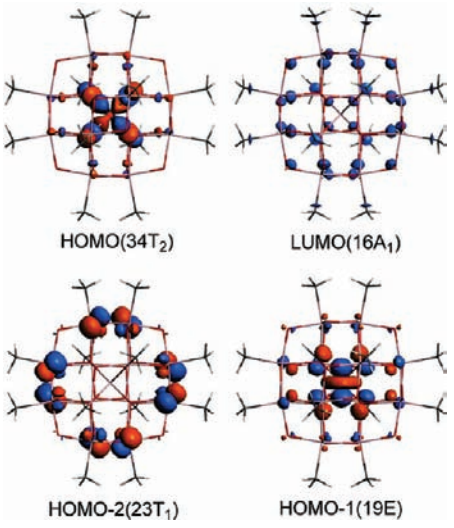

Figure 3. FMOs of ε-$[(MnO_4)Me_{12}Sb_{12}O_{24}]^{6-}/T_d$. Those of the α, β, γ, and δ structures are provided in the SI.

some primary differences between the two kinds of species, as summarized in $\{MeSbO_5\}$ and $\{WO_6\}$, the elementary octahedral building units of the respective $MnSb_{12}$ and PW_{12}. As seen from Figure 4, (i) horizontally, the Sb−O_b bond is always longer (~0.1 Å) and weaker (~0.1, Mayer indexes) than W−O_b, showing the lower bonding capability of Sb than W and the higher flexibility of the $MnSb_{12}$ framework than the PW_{12} framework; (ii) axially, the apical Sb−C is a weak single bond with a very long distance (2.214−2.240 Å; bond order of 0.44−0.48), in sharp contrast to the strong double W=O_t bond with a short distance (1.725−1.727 Å; bond order of 1.59−1.61), whereas in the opposite position, the interior Sb−O_i bond is significant shorter (2.202−2.291 Å of Sb−O_i vs 2.393−2.710 Å of W−O_i) and is obviously stronger than that of W−O_i (0.23−0.30 of Sb−O_i vs 0.13−0.15 of W−O_i, Mayer index),

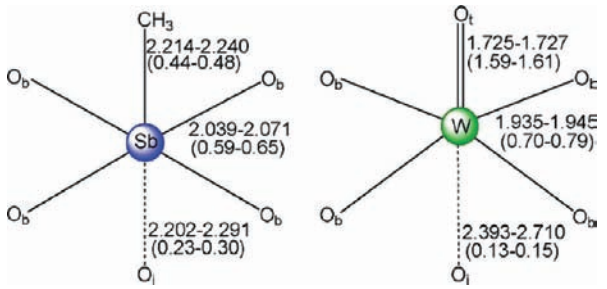

Figure 4. Bond lengths in building blocks of $[(MnO_4)Me_{12}Sb_{12}O_{24}]^{6-}$ and $[(PO_4)W_{12}O_{36}]^{3-}$. Mayer indexes are provided in parentheses.

exhibiting that the encrypted MnO_4^{2-} is more tightly bound to $Me_{12}Sb_{12}O_{24}$ than PO_4^{3-} is to $W_{12}O_{36}$. In reality, the divergence between $\{MeSbO_5\}$ and $\{WO_6\}$ originates the general difference of the valence orbital sets between the main-group and transition-metal elements.[32] As shown in Figure 5, in an approximately octahedral field tin makes use of 5s, 5p, and 5d orbitals (d^2sp^3 hybridization), while tungsten utilizes 5d, 6s, and 6p orbitals (d^2sp^3 hybridization) in forming σ bonds. NBO analysis clearly exhibits that the low-energy E_g orbitals ($5d_{x^2-y^2}$, $5d_{z^2}$) of tungsten are notably active in the participation of chemical bonding, in contrast to the inactive high-energy E_g orbitals ($5d_{x^2-y^2}$, $5d_{z^2}$) of tin. Specifically, in the high oxidation state, the d-block W^{VI} is a very good π acceptor (empty T_{2g} orbitals) and tends to form horizontal W−O_b and, in particular, axial W=O_t π bonds, whereas the p-block Sb^V is a poor π acceptor and does not form extra π bonds and thus has low bonding capability. It has been suggested that the formation of M=O_t (Mo^{VI}, W^{VI}, V^V, etc.) in POMs is the main reason for the assembly of discrete polyanions,[2] and the weakness of the internal M−O_i bonds stems from the strong trans influence of the M=O_t interactions.[33] In comparison, the filling of the inorganic ligand at the terminal positions does not yield an obvious trans influence in $\{MeSbO_5\}$, as evaluated by the bond order ratio of Sb−C/Sb−O_i, e.g., 1−2 versus 11−13 of W=O_t/W−O_i in PW_{12}. This primary difference may be answered for the low cluster-forming propensity of tin. In addition, owing to the inactivity of Sb 5d orbitals, the lowest unoccupied molecular orbitals (LUMOs) of $MnSb_{12}$ are dominated by O p and C p nonbonding bands (Figure 3), in contrast to the W d_{xy}−O p π-antibonding bands in the LUMOs of PW_{12}.[34]

(32) Landis, C. R.; Cleveland, T.; Firman, T. K. *J. Am. Chem. Soc.* **1998**, *120*, 2641–2649.
(33) Anastasi, A. E.; Deeth, R. J. *J. Chem. Theory Comput.* **2009**, *5*, 2339–2352.
(34) Bridgeman, A. J.; Cavigliasso, G. *J. Phys. Chem. A* **2001**, *105*, 7111–7117.

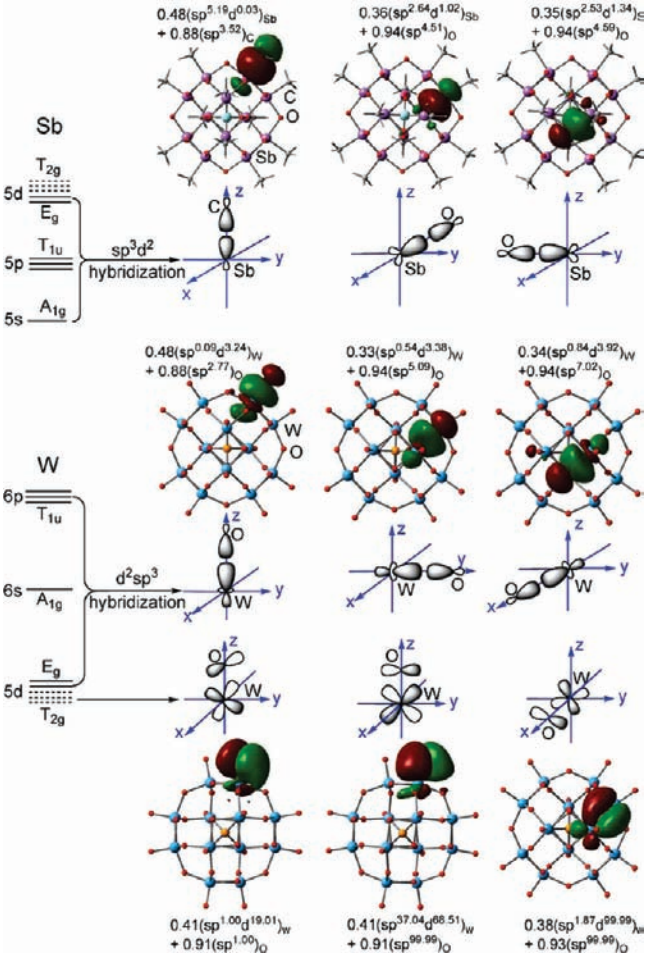

Figure 5. Schematic orbital diagrams of tin and tungsten in an octahedral environment and 3D representations of NBOs of ε-$[(MnO_4)Me_{12}Sb_{12}O_{24}]^{6-}$ and ε-$[(PO_4)W_{12}O_{36}]^{3-}$. Mn^{II} is replaced by Zn^{II} to avoid NBO computational failure at the B3LYP level. The weak Sb−O_i and W−O_i bonds cannot be detected.

Relative Stability. Our calculations show the growing stability order of $\alpha < \beta < \gamma < \delta < \varepsilon$ (ΔE_t; Table 2), which differs strikingly from that of the classical Keggin POMs. β-$MnSb_{12}$, obtained by a 60° rotation of one $\{(MeSb)_3O_6\}$ triad of the α isomer, gains 3.57 kcal/mol in stability. When two or more triads are rotated, an edge-sharing $[Sb_2(\mu\text{-}O)_2Me_2]$ dumbbell (denoted as $\{Sb_2\}$) appears. The γ, δ, and ε isomers, with 1, 3, and 6 $\{Sb_2\}$, respectively, are of substantially lower energy (−18.48 to −69.60 kcal/mol) than the α structure, with an energy decrease of ∼12 kcal/mol *per* $\{Sb_2\}$ on average. Conversely, for the classical $[PW_{12}O_{40}]^{3-}$, the order obtained at the mPWPW91/TZP level is $\alpha > \beta > \gamma > \delta > \varepsilon$ (Table SI4 in the SI), in well agreement with the recent study of López and Poblet.[7] It has been suggested that the edge-sharing unit embedded in the classical γ, δ, and ε Keggin structures is destabilizing, presumably arising from the electrostatic repulsion caused by a short M^{VI}−M^{VI} contact.[4] In reality, we found that γ-, δ-, and ε-$[PW_{12}O_{40}]^{3-}$ are notably enhanced (16.32−56.42 kcal/mol) compared to the α and β isomers, with an energy increase of ∼9.0 kcal/mol *per* $[W^{VI}{}_2(\mu\text{-}O)_2O_2]$ fragment (denoted as $\{W_2\}$). Hence, despite a great similarity in the structures, the $\{Sb_2\}$ and $\{W_2\}$ fragments seem to play opposite roles in the assembly of $MnSb_{12}$ and PW_{12}, respectively.

Table 2. Six Kinds of Relative Bonding Energies[a] (kcal/mol) of Five $[(MnO_4)Me_{12}Sb_{12}O_{24}]^{6-}$ Isomers

anions	ΔE_t	ΔE_{free}	ΔFIE	ΔDE (ΔDE$_{host}$/ΔDE$_{guest}$)
α/T_d	0.00	0.00	0.00	0.00 (0.00/0.00)
β/C_{3v}	−3.57	−14.07	2.45	8.05 (+9.71/−1.66)
γ/C_{2v}	−18.48	−25.36	0.84	6.04 (+13.60/−7.56)
δ/C_{3v}	−42.36	−33.54	−14.23	5.41 (+16.05/−10.64)
ε/D_2	−69.60	−43.57	−40.73	14.72 (+28.88/−14.16)
ε/T_d	−69.50	−43.59	−40.46	14.60 (+28.76/−14.16)

[a] Defined as the energy of α subtracting that of the others, and negative values denote favorable energies.

It is noteworthy that we previously have observed this kind of unusual stability order in 12-electron-reduced POMs and polyoxothiometalate anions,[16] in which the preference in the formation of the ε, δ, and γ anions can be easily attributed to the very stable $[M^V{}_2(\mu\text{-}O)_2O_2]$ (X = O, S; M = Mo) subunit with a single metal−metal σ bond formed inside. In contrast, the Sb^V−Sb^V distance inside $\{Sb_2\}$ is significantly long (computed as 3.156−3.183 Å and experimental 3.09−3.21 Å vs ∼2.99 Å of a normal single bond[31]), and no Sb−Sb bond is present, as substantiated by both a very low bond order (∼0.10, Mayer index) and AIM analysis (no bond critical point between two tin ions[35]). Apparently, this property is still similar to that of the $\{W^{VI}{}_2\}$ fragment without the W−W bond (∼0.10, Mayer index; Figure SI2 in the SI) in the oxidized γ-, δ-, and ε-PW_{12} structures. Note, in particular, that the p-block Ga^{3+} (0.62 Å) and Al^{3+} (0.535 Å)[31] with ionic radii similar to that of Sb^{5+}/W^{6+} (0.60 Å) are also preferred to assemble ε-Keggin,[10,11] $[M_{13}O_4(OH)_{24}(H_2O)_{12}]^{7+}$, in which water ligands fill the terminal positions on the surface and hydroxyl groups occupy the bridging sites. Also, no Ga−Ga or Al−Al bond (Mayer index <0.05; computed 2.926 and 3.046 Å for M = Al and Ga,[36] respectively) is formed inside the binuclear $[M^{III}{}_2(\mu\text{-}OH)_2(H_2O)_2]$ (M = Al, Ga). Lippard and co-workers[17] suggested that for these complexes the short M−M contact inside the edge-sharing fragment can be rationalized by lowered electrostatic repulsion between the two lowly charged metal ions, versus the highly charged M^{6+} metal ions in POMs. Indeed, in comparison to the $\{W^{VI}{}_2\}$ of PW_{12}, besides the longer distance of Sb−Sb (calculated 3.157−3.183 Å of Sb−Sb vs 2.992−3.023 Å of W−W), the charge of Sb^{5+} inside $\{Sb^V{}_2\}$ is ∼0.5 smaller (2.812−2.861 of Sb^{5+} vs 3.356−3.394 of W^{6+}) in $MnSb_{12}$.

Evidently, lowering of the Sb−Sb repulsion is not sufficient but is necessary to explain the preferred formation of the edge-sharing fragment embedded in the antimonates. To further evaluate the stabilization behavior of $\{Sb_2\}$, we decompose each of the isomeric structures into 12 octahedral building blocks, in which all four O_b atoms are terminated by hydrogen atoms added along the initial boundary O_b−Sb bonds,[37]

(35) Bader, R. F. W. *Atoms in Molecules—A Quantum Theory*; Oxford University Press: Oxford, U.K., 1990. The free software XAIM obtained from http://www.quimica.urv.es/XAIM/ is used to perform Bader analysis.

(36) Solvent (water) effects are considered using conductor-like screening model (COSMO) in the optimization process at the mPWPW91/TZP level.

(37) The bond lengths of all O−H's in $[MeSb(OH)_5]^-$ are optimized under constraints of all of the other parameters. Then, a positive point charge of 0.60 is added in the mean positions of the initial two tin atoms inside the same triad to calculate the single-point energy. The bond order of Sb−O_i is adjusted via the magnitude of the point charge (+0.60), and the obtained 0.24−0.28 falls in the range of 0.23−0.30 observed in the overall $MnSb_{12}$ anion. The O−H bond with a fixed distance of 0.97 Å also gives a good result. Detailed steps are given in Figure SI1 in the SI.

Table 3. Bonding Energies (au) of $[MeSb(OH)_5]^{0.40-}$ for Five $[(MnO_4)Me_{12}Sb_{12}O_{24}]^{6-}$ Isomers

anions	1[a]	2	3	4	average
α/T_d	−3.03000				−3.03000 (0.00[b])
β/C_{3v}	−3.03530	−3.03092	−3.02983		−3.03174 (−1.09)
γ/C_{2v}	−3.03921	−3.03298	−3.03654	−3.032267	−3.03437 (−2.74)
δ/C_{3v}	−3.03792	−3.03339	−3.03777		−3.03675 (−4.24)
ε/T_d	−3.03740				−3.03740 (−4.64)

[a] The numbers 1−4 denote the different kinds of building blocks in the structure as labeled in Figure 1. [b] Relative energies (kcal/mol). Negative values denote favorable energies.

simply simulating the chemical environment of the overall anion. The treatment of the internalized MnO_4^{6-} is difficult because of its 12-coordinate number as well as its relatively weak interaction to an individual addendum. Herein, the hydrogen atom is still used and added along the initial O_i−Mn bond. Specifically, a positive point charge (+0.60) is placed near the interior O_i with a distance of 1.00 Å,[37] aimed to mimic the Sb−O_i interaction. The resulting octahedron is $[MeSb(OH)_5]^{0.40-}$ and is abbreviated as {Sb}. For the T_d-symmetric α or ε form, only one kind of building block is present and more types appear when the symmetry of the isomer is lowered, e.g., three of β/C_{3v} and δ/C_{3v} and four of γ/C_{2v}, respectively. By this approach, it is found that the building units of the $MnSb_{12}$ isomers are stabilized in the order α < β < γ < δ < ε on average (Table 3), reproducing very well the trend of the overall structures (ΔE_t). Interesting details are emerging when scrutinizing individual data. For instance, the most stable octahedron is not from the most stable ε isomer but from the edge-sharing $\{Sb_2\}$ unit in the γ structure (γ_1, the subscript denotes the position of the unit in the structure, as labeled in Figure 1), while the least stable unit is not from the least stable α isomer but from the nonrotated triad at the bottom triad of the β form (β_3) despite their very close energies; the enhanced stability of the β structure over the α one originates primarily from the contributions of the three octahedra inside the upper $\{(MeSb)_3O_6\}$ triad (β_1; Figure 1), which is 60° rotated from the α isomer; the noticeable decreasing stability of the octahedra from edge-sharing $\{Sb_2\}$ with the order γ_1 (0.00 kcal/mol) > δ_1 (0.81) > ε (1.14) can be attributed to the increasing crowding of $\{Sb_2\}$ in the structure, etc. More importantly, two key points can be drawn from the values in this table: (i) For all of $MnSb_{12}$ studied, the octahedron of $\{Sb_2\}$ is generally more stable than others, and (ii) for a given structure with $\{Sb_2\}$, the most stable octahedron is always from this fragment. Thus, it is clear that the $\{Sb_2\}$ fragment actually exerts a stabilizing effect, via its favorable octahedral components rather than itself as an indivisible unit. Note that there is no metal−metal contact inside a single octahedron and the electrostatic repulsion cannot, therefore, be taken as direct evidence to explain the behavior of $\{Sb_2\}$. Interestingly, besides those from $\{Sb_2\}$, there are some other kinds of favorable units, e.g., the one from the lower triad of δ (δ_3; Figure 1), being 0.23 kcal/mol more stable than that of the ε structure (δ_3 > ε).

(38) The bond lengths of all O−H's in $[O_t{=}W(OH)_5]^-$ are optimized under the constraints of all of the parameters. The energy of the building block is obtained after a positive point charge of +0.65 is added in the mean positions of the initial two tungsten atoms inside the same triad. The calculated bond order W−O_i (~0.14) falls in the range of 0.13−0.15 observed in the overall PW_{12} anion. The O−H bond with a fixed distance of 0.97 Å also gives a good result.

However, what is the situation of $\{M_2\}$ in classic Keggin anions? For further comparison and confirmation, a similar building block decomposition approach is also performed on the five isomeric PW_{12} structures, and the positive point charge is set to 0.65.[38] The data obtained are provided in Table SI5 in the SI. Interestingly, the energy of $[O_t{=}W(OH)_5]^{0.35-}$ (abbreviated as {W}) destabilizes in the order β < α < γ < δ < ε, reproducing well the trend of the Keggin anions. Besides providing useful information, two key structural features can be drawn from the table: (i) for all of PW_{12}, the octahedron of $\{W_2\}$ is always less stable than others, and (ii) for structures with $\{W_2\}$, the least stable octahedron is invariably from this fragment. Apparently, all of the data support the destabilizing effect of the edge-sharing $\{W_2\}$, which tends to reduce the overall stability via its disfavored building blocks. Also, noticing the absence of the metal−metal contact in the single building block, the instability of the $\{W_2\}$ fragment thus cannot be described by the W^{VI}−W^{VI} electrostatic repulsion. Actually, for a given stable Keggin-type structure, all of the octahedral components were fully relaxed to its maximum conformation under the constraint of the surrounding environment. Consequently, the electrostatic repulsion between the short-contact metal ions inside the $\{M_2\}$ fragment is well dispersed, for the classical tungstates and antimonates as well. Hence, despite opposite effects of the edge-sharing $\{M_2\}$ fragments in the assembly of $MnSb_{12}$ and PW_{12}, their similar origin sheds new insight into the nature of the two different kinds of complexes.

The building block decomposition approach validates the reversed behavior of the $\{Sb_2\}$ and $\{W_2\}$ fragments. However, the underlying reason remains unclear and has to be brought forward. This issue can be rationalized via systematical examination of the structural parameters of each octahedral unit including bond lengths of M−O_b and M−O_i and angles of O_b−M−O_b, M−O_b−H, Y−M−O_b (Y = C and O_t for M = Sb and W, respectively), etc. The data of $MnSb_{12}$ obtained (Table SI7 in the SI) are shown in Figure 6, where peaks and valleys are energetically favored and disfavored, respectively. Among the five kinds of parameters, the angles of C−Sb−O_b and O_b−Sb−O_b, and the bond length of Sb−O_i are closely related to the octahedral bonding environment of the metal center. The distinct dependences of the {Sb} energy (E_{Sb}) on the three parameters, including its direct relationship with C−Sb−O_b (E_{Sb} ~ sum of C−Sb−O_b; Figure 6b) and Sb−O_i (E_{Sb} ~ Sb−O_i; Figure 6e) and its inverse relationship with O_b−Sb−O_b (E_{Sb} ~ 100/sum of O_b−Sb−O_b; Figure 6c), are combined to suggest that the Sb ion is too close to the four O_b planes, as visualized directly by the very close 90° of the four O_b−Sb−O_b (89.55−89.91°, on average) and four C−Sb−O_b (93.18−95.34°, on average) angles. It is also noteworthy that the interior Sb−O_i bond is not quite different from the terminal Sb−C bond, including the bond length and strength (2.202−2.291 vs 2.214−2.240 Å and 0.23−0.30 vs 0.44−0.48 of the Mayer index); i.e., {Sb} retains a relatively regular octahedron in all $MnSb_{12}$ structures. This primary structural feature becomes clearer when the distance from the tin to the four-O_b plane (Sb → 4O_b) is examined, e.g., besides the very small values (0.116−0.160 Å[39]), which manifests that the tin ion and all four bridging

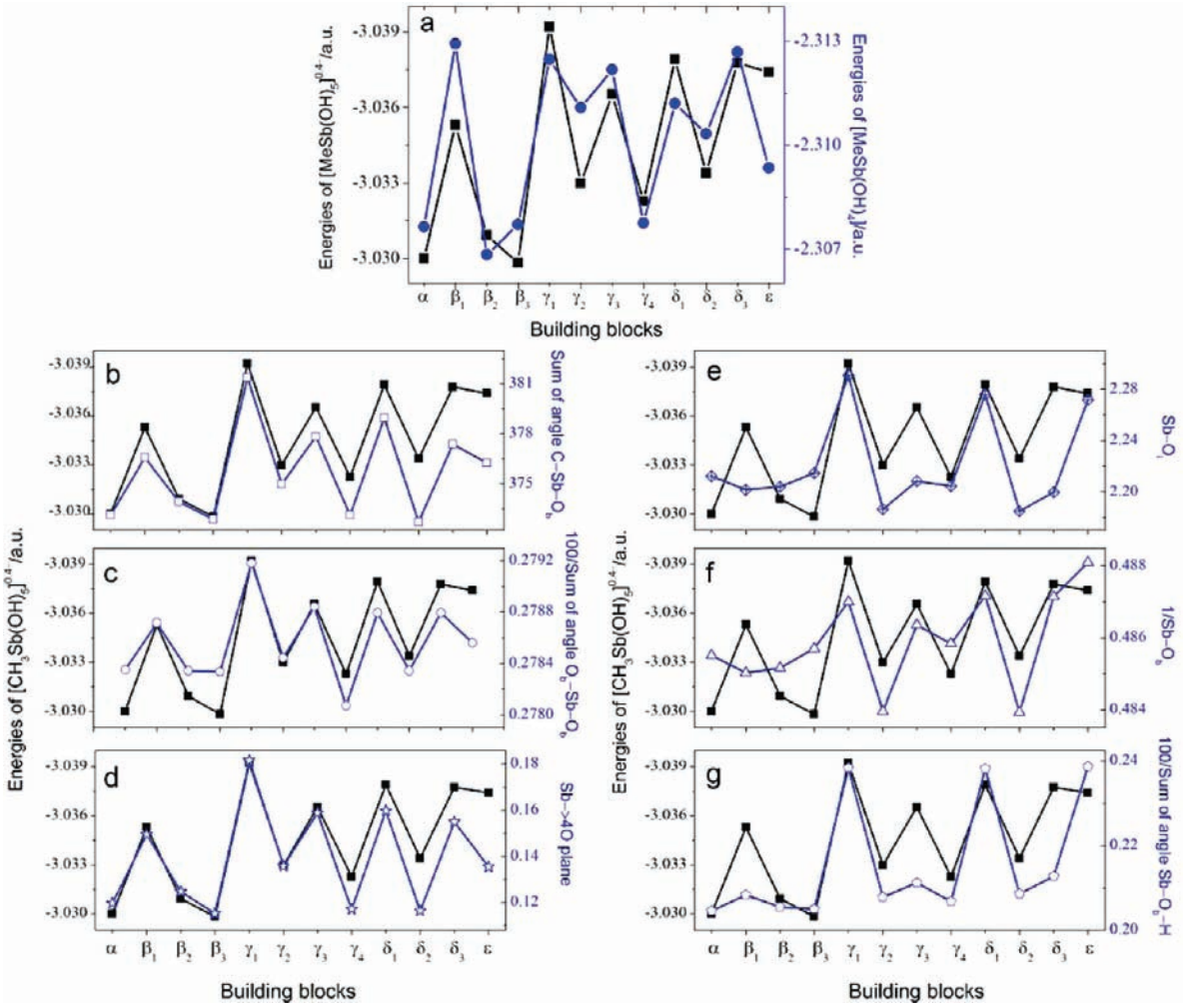

Figure 6. Dependences of the $[MeSb(OH)_5]^{0.4-}$ and $[MeSb(OH)_4]$ energies on six kinds of structural parameters. Negative values denote favorable energies. An average bond length of Sb−O_b is used. Energetic data of $[MeSb(OH)_4]$ are provided in Table SI6 in the SI.

oxygen atoms are nearly coplanar, its direct proportion with E_{Sb} ($E_{Sb} \sim$ Sb → 4O_b; Figure 6d) suggests that the {Sb} octahedron is compressed along the axial direction. Simultaneously, the inverse relationship of the Sb−O_b bond length ($E_{Sb} \sim 1$/Sb−O_b; Figure 6f) with E_{Sb} also implies that the octahedron is elongated in the horizontal direction. In the case of the Sb−O_b−H angle, which corresponds to the Sb−O_b−Sb linker in the overall structure, the decreasing tendency ($E_{Sb} \sim 100$/sum of Sb−O_b−H; Figure 6g) can be attributed to the enhanced repulsion between the two lone pairs in the oxygen atom when the bond angle increases, e.g., large 104.9−122.2° herein versus 104.5° in water.

Upon scrutiny of the building block structures of the five PW_{12} isomers, it is not surprising that the five $MnSb_{12}$ isomers have such a peculiar stability order. As provided in Table SI8 in the SI and as shown in Figure 7, the dependences of the {W} energy (E_W) on all six kinds of parameters are perfectly reversed from those observed in {Sb}. For instance, the relationships between E_W and three parameters, including the inverse relationship with the O_t−W−O_b angle ($E_W \sim 100$/sum of O_t−W−O_b; Figure 7b) and the W−O_i bond length ($E_W \sim 1$/W−O_i; Figure 7e) and the direct relationship with the O_b−W−O_b angle ($E_W \sim$ sum of O_b−W−O_b; Figure 7c), are combined to suggest that the tungsten ion is too far from the four-O_b plane. The feature can be further substantiated by the distance from the tungsten to the four-O_b plane (W → 4O_b), including both the significant larger value (0.357−0.425 Å[39]) than that of Sb → 4O_b (0.116−0.160 Å) and its negative relationship with E_W ($E_W \sim 1$/W → 4O_b; Figure 7d). On the other side, the positive relationship of the W−O_b bond length ($E_W \sim$ W−O_b; Figure 7f) with E_W indicates that the octahedron is also compressed in the horizontal direction. The W−O_b−H angle in {W} corresponds (and equals) to the W−O_b−W linkage in the PW_{12} structure. In contrast to the small Sb−O_b−H angle (104.9−122.2°) with a reducing tendency ($E_{Sb} \sim 1$/sum of Sb−O_b−H; Figure 6g), the W−O_b−H angle is large (115.8−139.2°) and tends to increase ($E_W \sim$ sum of W−O_b−H; Figure 7g). It is found that the transition metal generally prefers a large M−O_b−M angle because of the favorable π-type interaction between metal d and bridging O p orbitals.[34] In the case of the octahedral model with terminal hydrogen atoms, the W d−O p π-bonding nature in W−O_b is retained and the inclination of W−O_b−H

(39) (a) Schomaker, V.; Waser, J.; Marsh, R. E.; Bergman, G. *Acta Crystallogr.* **1959**, *12*, 600–604. (b) Scheringer, C. *Acta Crystallogr.* **1971**, *B27*, 1470−1472. The source code of the least-squares best-fit plane is obtained free of charge from http://www.bmm.icnet.uk/people/suhail/plane.html.

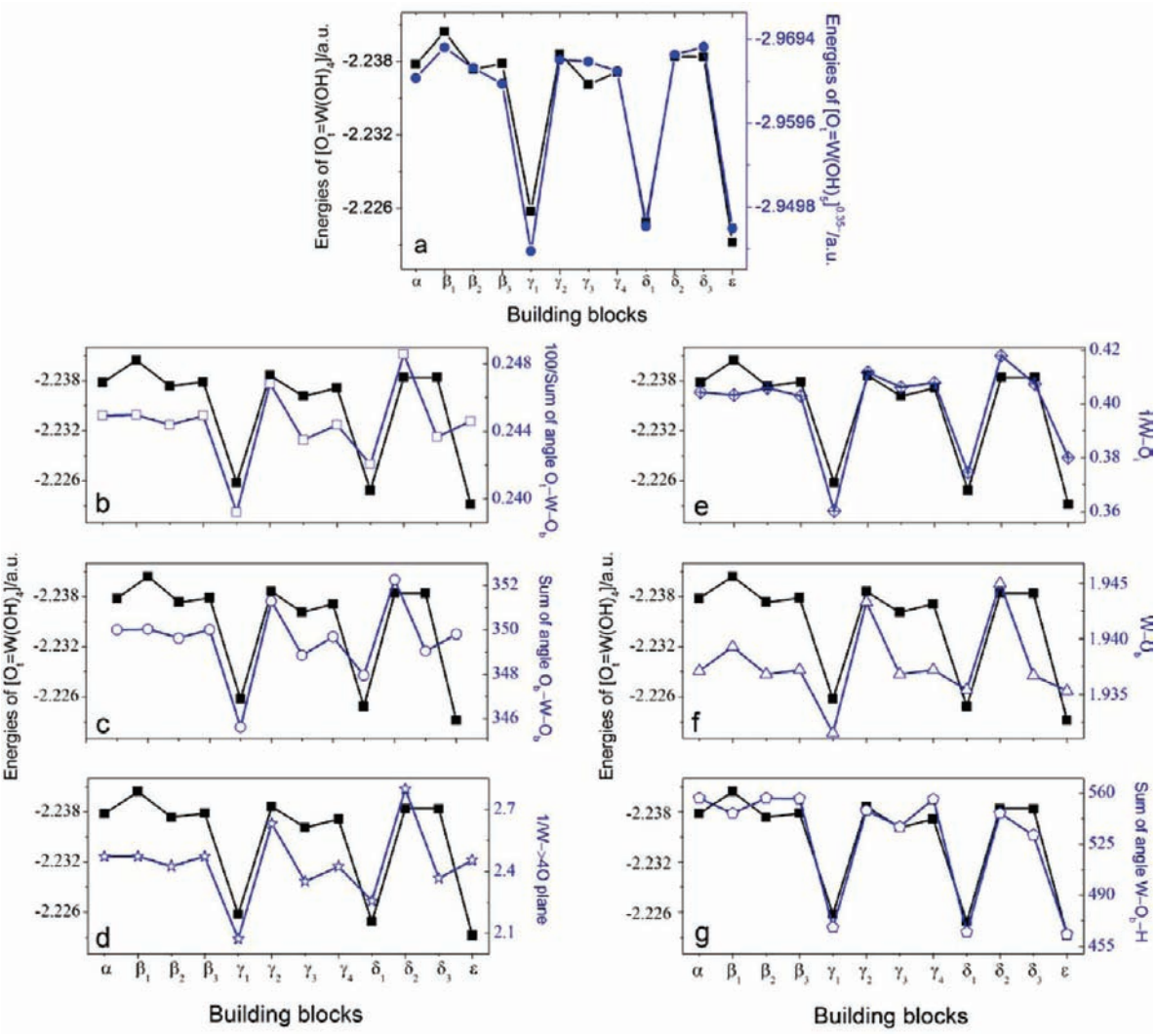

Figure 7. Dependences of the $[O_t{=}W(OH)_5]^{0.65-}$ and $[O_t{=}W(OH)_4]$ energies on six kinds of structural parameters. Negative values denote favorable energies. An average bond length of W−O_b is used. The energy of $[O_t{=}W(OH)_4]$ (Table SI8 in the SI) instead of $[O_t{=}W(OH)_5]^{0.65-}$ is used in the plot because of its good relationship with the structural parameters.

to a large value is maintained. In addition, the σ and π characters in the W−O_b bond may enhance the change transferring from O^{2-} to a highly charged W^{6+} ion, and the reduced repulsion between the lone pairs in the oxygen atom is another possible cause.

Host−Guest Energy Analysis. To delve further into the difference between the $MnSb_{12}$ and PW_{12} isomers, additional energy analysis is needed. The clathrate model[40] provides a simple but useful means for qualitatively exploring the properties of these host−guest complexes, on the basis of which the energy of $MnSb_{12}$ can be decomposed as follows.

$$MnO_4{}^{6-}(\text{free}) + Me_{12}Sb_{12}O_{24}(\text{free}) \rightarrow MnO_4{}^{6-}@Me_{12}Sb_{12}O_{24} \quad (1)$$

The energy differences of the five anions can be evaluated using

$$\Delta E_t = \Delta E_{host}(\Delta E_{free}) + \Delta DE(\Delta DE_{guest} + \Delta DE_{host}) + \Delta FIE \quad (2)$$

where E_t is the energy of the optimized anion, E_{free} is the sum of energies of the fully relaxed $Me_{12}Sb_{12}O_{24}$ (E_{host})[41] and $MnO_4{}^{6-}$ (E_{guest}), DE is the sum of the deformation energies of the host and guest from their fully relaxed conformations (DE_{guest} + DE_{host}), and FIE is the host−guest interaction between $Me_{12}Sb_{12}O_{24}$ and $MnO_4{}^{6-}$. The prefix "Δ" denotes the energy difference between β, γ, δ, and ε and the reference α one. Note that all of the structures share the same guest anion; ΔE_{free} is thus the difference between the free hosts (ΔE_{host}). The computed data are given in Table 2 and plotted in Figure 8, where negative values denote disfavored energies. Several points can be drawn from these values. First, the difference in the spatial arrangement of the host (ΔE_{host} or ΔE_{free}) is the most important factor governing the relative stability of the anions (ΔE_t). Besides the dominant contribution in the δ and ε structures ($\Delta E_{host} = -33.54$ kcal/mol vs

(40) Day, V. W.; Klemperer, W. G. *Science* **1985**, *228*, 533–537.

(41) All of the cages are optimized under constraints of their ideal symmetry. For γ-$Me_{12}Sb_{12}O_{24}$ and γ-$W_{12}O_{36}$, four neodynium atoms are included and located at the initial positions of the interior oxygen atoms to avoid structural collapse during the optimization process. Single-point energies are used and obtained based on the empty structures.

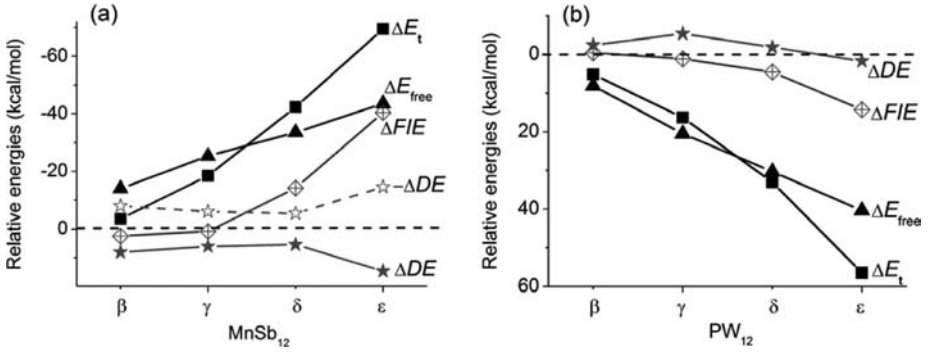

Figure 8. Five kinds of relative energies as functions of five $[(MnO_4)Me_{12}Sb_{12}O_{24}]^{6-}$ (a) and $[(PO_4)W_{12}O_{36}]^{3-}$ (b) isomers.

$\Delta E_t = -42.36$ kcal/mol for δ and $\Delta E_{host} = -43.57$ kcal/mol vs $\Delta E_t = -69.60$ kcal/mol for ε), ΔE_t of β and γ originates completely from this term. Second, the influence of the host−guest interaction (ΔFIE) is important. Despite the very large absolute data of FIE (−1436.49 to −1479.67 kcal/mol; Table SI10 in the SI) that may account for the assembly of the entire host−guest structure, the differences among the five isomers are not so significant. For instance, the former three isomers including the α, β, and γ structures share very close ΔFIE (0.00−2.45 kcal/mol), and in these cases, ΔFIE is minor and can be nearly neglected. Differently, for the later stable δ and ε structures, ΔFIE increases considerably (−14.23 to −40.73 kcal/mol) and becomes an important contributor to the enhanced ΔE_t. Third, deformation of the structure (ΔDE) is another principal factor. ΔDE has two components: the guest (ΔDE_{guest}) and the host (ΔDE_{host}). As listed in Table 2, the steadily increased stability of the guest (ΔDE_{guest}) with order $\alpha < \beta < \gamma < \delta < \varepsilon$ agrees nicely with that of the increased inner cavity of the structure. Conversely, the neutral host cage with very large deformation (179.82−208.70 kcal/mol of DE_{host} vs 0.70−14.86 kcal/mol of DE_{guest}; Table SI10 in the SI) exhibits a continuously decreased pattern ($\alpha > \beta > \gamma > \delta > \varepsilon$; Figure 8a), reflecting that the more stable cage is always more distorted under the influence of the guest anions. As expected, the deformation between the host cages is always significant (0.00−28.88 kcal/mol of ΔDE_{host} vs 0.00∼−14.16 kcal/mol of ΔDE_{guest}) and thus results in the negative contribution of ΔDE to ΔE_t, and, on the other hand, its influence is partly reduced because of the bucking effects of ΔDE_{guest}. In summary, in all cases, ΔE_{host} is dominant while ΔDE and ΔFIE are subordinate, and the negative ΔDE is the principal factor to reduce ΔE_t. In the case of the five PW_{12} isomers, despite the inverse stability order, comparable results are obtained based on the same decomposition method.[42] The difference observed comes from the low charge of the PO_4^{3-} anion, which yields much smaller host−guest interaction (FIE, −537.70 to −552.42 kcal/mol; Table SI11 in the SI) and structural distortion (DE, 50.04−57.14 kcal/mol), as compared to the large values in $MnSb_{12}$. Consequently, ΔFIE (0.00−14.32 kcal/mol; Table SI4 in the SI) and ΔDE (−5.35−1.75 kcal/mol) are less important, and the spatial arrangement (ΔE_{host} with $\alpha > \beta > \gamma > \delta > \varepsilon$, 0.00−40.33 kcal/mol) turns out to be the most dominant factor governing the relative stability of the PW_{12} isomers (ΔE_t, 0.00−56.42 kcal/mol; Figure 8b).

(42) PO_4^{3-}(free) + $W_{12}O_{36}$(free) → PO_4^{3-}@$W_{12}O_{36}$

Given the large differences of MnO_4^{6-} and PO_4^{3-} in charge and size as well as the resulting dissimilarities of FIE/DE (or ΔFIE/ΔDE) in the $MnSb_{12}$ and PW_{12} structures, one may doubt that the encapsulated moieties play essential roles in their inverted stability order. The hypothetical neutral cages, $Me_{12}Sb_{12}O_{24}$ and $W_{12}O_{36}$, the extreme states of two kinds of complexes, are probably the best examples to elucidate such an issue. Evidently, in the absence of guest molecules, the two kinds of cages have exhibited their innately inverse order (ΔE_{free} in Figure 8; $\alpha < \beta < \gamma < \delta < \varepsilon$ of $Me_{12}Sb_{12}O_{24}$ and $\alpha > \beta > \gamma > \delta > \varepsilon$ of $W_{12}O_{36}$, respectively), completely ruling out the possible influence of the guest anion. Detailing the relationship between the structural parameters and the energies of the building blocks assembled in the cages advances our understanding of their quite different nature. As expected, the energy/structure pattern observed in the blocks of PW_{12} is also preserved in those of free $W_{12}O_{36}$ (Figure SI3 in the SI), including the direct relationship of E_W (energy of $[O_t{=}W(OH)_4]$) with the angles of $O_b{-}W{-}O_b$ ($E_W \sim$ sum of $O_b{-}W{-}O_b$) and $W{-}O_b{-}H$ ($E_W \sim$ sum of $W{-}O_b{-}H$) and the inverse relationship of E_W with the angle $O_t{-}W{-}O_b$ ($E_W \sim 100$/sum of $O_t{-}W{-}O_b$) and the distance of $W \rightarrow 4O_b$ ($E_W \sim 1/W \rightarrow 4O_b$). However, the dependence of E_W on the $W{-}O_b$ distance becomes obscure. There is no doubt that the $\{W_2\}$ fragment exerts a destabilizing effect, via its two disfavored building components (Table SI12 in the SI). By contrast, a very loose energy/structure pattern with an apparent divergence is observed in the components of the $Me_{12}Sb_{12}O_{24}$ cages (Figure SI3 in the SI), and that might be attributed to the structural disparities between the pyramidal tin ion in the cages and the octahedral tin ion in the anions. Detailed analysis shows that the positive relationship of E_{Sb} (energy of $[MeSb(OH)_4]$) with the $C{-}Sb{-}O_b$ angle ($E_{Sb} \sim$ sum of $C{-}Sb{-}O_b$) and the $Sb \rightarrow 4O_b$ distance ($E_{Sb} \sim Sb \rightarrow 4O_b$) and the negative relationship of E_{Sb} with the $Sb{-}O_b{-}H$ angle ($E_{Sb} \sim 1/$sum of $Sb{-}O_b{-}H$) observed in $MnSb_{12}$ are partly retained, while the dependences of E_{Sb} on the $O_b{-}Sb{-}O_b$ angle and $Sb{-}O_b$ distance are broken. However, the stabilizing effect of the $\{Sb_2\}$ fragment is doubtless and that does come from its disfavored building components (Table SI13 in the SI).

Despite the disorders of several parameters, the qualitatively opposite trends of the $Y{-}M{-}O_b$ (Y = C or O_t) and $M{-}O_b{-}M$ angles and the $M \rightarrow 4O_b$ distance with building unit energy in $Me_{12}Sb_{12}O_{24}$ and $W_{12}O_{36}$ cages explicitly reflect the inherent difference between the two species. Similar to those observed in the anions, the positive

relationships of C−Sb−O_b and Sb → 4O_b with E_{Sb} suggest that [MeSb(OH)$_4$] in $Me_{12}Sb_{12}O_{24}$ is compressed in the axial direction, despite their significant increase in the absence of the guest anion (100.0−104.1° in the cage vs 93.18−95.34° in $MnSb_{12}$ of C−Sb−O_b, on average; 0.350−0.463 Å in the cage vs 0.115−0.182 Å in $MnSb_{12}$ of Sb → 4O_b), whereas the [O_t=W(OH)$_4$] in $W_{12}O_{36}$ is further elongated axially (105.6−107.6° in the cage vs 100.6−104.5° in PW_{12} of O_t−W−O_b, on average; 0.520−0.583 Å in the cage vs 0.357−0.482 Å in PW_{12} of W→4O_b), and this is expected because of the absent attraction of negative guests encapsulated inside. In the case of the horizontal M−O_b−M angle, the data are notably increased in all of the free cages as compared to those in the anions (123.4−148.0° in the cage vs 115.8−139.2° in PW_{12}; 115.4.3−134.8° in the cage vs 104.8−122.2° in $MnSb_{12}$, on average), and as a direct consequence, W−O_b−W becomes more and Sb−O_b−Sb less favorable, respectively. Thus, apart from regulating the parameters to energy, the inclusion of the guest anion in the cages yields opposite influences on the two species, i.e., axially reducing the elongation trend in PW_{12} but enhancing compression in $MnSb_{12}$ and horizontally increasing M−O_b−M in PW_{12} but decreasing the M−O_b−M angle in $MnSb_{12}$.

In reality, the overall stability has a small relationship with the charged guest because of the strong effects of the edge-sharing fragment. For instance, for the oxidized Keggin tungstates with rigid frameworks, $\alpha > \beta > \gamma > \delta > \varepsilon$ is also held by highly charged Keggin anions $[(XO_4)W_{12}O_{36}]^{n-}$ (X = Si, Ge, Al, Ga, Zn, Mn; n = 4−6; Table SI14 in the SI). In particular, the α/β-[(AlO_4)-$W_{12}O_{36}]^{5-}$ and α/β-$[(GaO_4)W_{12}O_{36}]^{5-}$ differences calculated agree very well with the experimental data (2.08 vs 2.1 + 0.5[6a] kcal/mol for X = Al; 1.29 vs 0.65 kcal/mol[6c] for X = Ga), validating our computational method. As for the Keggin antimonites with flexible frameworks, $\alpha < \beta < \gamma < \delta < \varepsilon$ is held in $[(ZnO_4)Me_{12}Sb_{12}O_{24}]^{6-}$ (Table SI15 in the SI). In the case of the hypothetical $[(PO_4)Me_{12}Sb_{12}O_{24}]^{3-}$ with low charge, the crossover of $\alpha > \beta$ is happened ($\beta < \alpha < \gamma < \delta < \varepsilon$; Tables SI15 and SI16 in the SI), coming from the larger deformation of the β cage than the α one. No doubt, the type as well as the charge of the guest anion exerts a fundamental influence to the overall structure;[43] nevertheless, it is only one of the factors to quantitatively tune the inherent properties of the cages.

Conclusions

The five Baker−Figgis isomers $[(MnO_4)Me_{12}Sb_{12}O_{24}]^{6-}$ (Me = CH_3), simplified models of the antimonate complexes in experiments, have been investigated at the level of DFT. Despite a significant resemblance with the classical Keggin anions in the structures, the nature of these complexes is quite unique, arising from the low bonding capacity of the 5d valence orbital sets of the main-group element tin. Simple building block decomposition and energy decomposition analysis are found to be very useful in illuminating the primary differences between two kinds of species. The calculations led to the following rules:

(1) The stability order of $[(MnO_4)Me_{12}Sb_{12}O_{24}]^{6-}$ is $\alpha < \beta < \gamma < \delta < \varepsilon$, which perfectly inverses to the well-known trend of the classical Keggin-type $[PW_{12}O_{40}]^{3-}$ anions.

(2) There are two primary structural differences between the two kind of species, including the small trans influence of the axial Sb−C bond and small Sb−O−Sb angle in $[(MnO_4)Me_{12}Sb_{12}O_{24}]^{6-}$, in shape contrast to the strong trans influence of the apical W=O_t bond and large W−O−W angle in $[PW_{12}O_{40}]^{3-}$.

(3) The building block decomposition clarifies the distinct effects of the edge-sharing fragment coming from its octahedral components rather than itself as an indivisible unit, including the stabilizing effect of $[Sb^{V}_2(\mu\text{-}O)_2(CH_3)_2]$ in $[(MnO_4)Me_{12}$-$Sb_{12}O_{24}]^{6-}$ and the destabilizing effect of $[W^{VI}_2$-$(\mu\text{-}O)_2O_2]$ in $[PW_{12}O_{40}]^{3-}$.

(4) Detailed parameter analysis unravels that the reversed stability order of $[(MnO_4)Me_{12}Sb_{12}$-$O_{24}]^{6-}$ and $[PW_{12}O_{40}]^{3-}$ stems from the inverted distorted behavior of their building units; i.e., the former is compressed in the axial direction and elongated in the radial direction, while the latter is compressed in the radial direction and elongated in the axial direction.

(5) Energy decomposition analysis suggests that the influence of the encapsulated anions on the overall anion is subordinate, and the difference in stability mainly lies in the different spatial arrangements of their cages.

The work has broad implications for understanding of the formation of non-POM Keggin-type species assembled by main-group elements, such as Al_{13}, Ga_{13}, and MAl_{12} (M = Ge^{IV}, Ga^{III}), which exhibit structural and electronic similarities with the antimonate complexes in this paper. Further studies on these compounds are in progress.

Acknowledgment. This work is supported by the National Natural Science Foundation of China (Grant 20775047). We thank Prof. Hai-Shun Wu and Prof. Xian-Ming Zhang for their dedication in NBO computation and analysis and the reviewers for constructive suggestions.

Supporting Information Available: Total bonding energies, Mayer indexes, Voronoi charges, Mulliken spin charges of Mn^{II}, energies and parameters of the building blocks of five $[(MnO_4)Me_{12}Sb_{12}O_{24}]^{6-}$ isomers; total bonding energies, relative energies, Mayer indexes, and parameters of the building blocks of five Keggin $[PW_{12}O_{40}]^{3-}$ isomers; bonding energies and parameters of the building blocks of five $Me_{12}Sb_{12}O_{24}$ and five $W_{12}O_{36}$ cages, selected NBOs, occupancies, orbital coefficients and hybrids, and orbital types of ε-$[PW_{12}O_{40}]^{3-}$ and ε-$[(MnO_4)Me_{12}Sb_{12}O_{24}]^{6-}$, figures of five kinds of structural parameters as functions of energies of [MeSb(OH)$_4$] and [O_t=W(OH)$_4$], and FMOs of α, β, γ, and δ structures. This material is available free of charge via the Internet at http://pubs.acs.org.

(43) Müller, A.; Kögerler, P. *Coord. Chem. Rev.* **1999**, *182*, 3–17.